Upper atmospheric gravity wave details revealed in nightglow satellite imagery

Steven D. Miller[a,1], William C. Straka III[b], Jia Yue[c], Steven M. Smith[d], M. Joan Alexander[e], Lars Hoffmann[f], Martin Setvák[g], and Philip T. Partain[a]

[a]Cooperative Institute for Research in the Atmosphere, Colorado State University, Fort Collins, CO 80523; [b]Cooperative Institute for Meteorological Satellite Studies, University of Wisconsin-Madison, Madison, WI 53706; [c]Atmospheric and Planetary Science, Hampton University, VA 23668; [d]Center for Space Physics, Boston University, Boston, MA 02215; [e]NorthWest Research Associates/Colorado Research Associates, Boulder, CO 80301; [f]Jülich Supercomputing Centre, Forschungszentrum Jülich, Jülich, Germany; and [g]Czech Hydrometeorological Institute, Satellite Department, Prague, Czech Republic

Edited by Mark H. Thiemens, University of California at San Diego, La Jolla, CA, and approved October 12, 2015 (received for review April 24, 2015)

Gravity waves (disturbances to the density structure of the atmosphere whose restoring forces are gravity and buoyancy) comprise the principal form of energy exchange between the lower and upper atmosphere. Wave breaking drives the mean upper atmospheric circulation, determining boundary conditions to stratospheric processes, which in turn influence tropospheric weather and climate patterns on various spatial and temporal scales. Despite their recognized importance, very little is known about upper-level gravity wave characteristics. The knowledge gap is mainly due to lack of global, high-resolution observations from currently available satellite observing systems. Consequently, representations of wave-related processes in global models are crude, highly parameterized, and poorly constrained, limiting the description of various processes influenced by them. Here we highlight, through a series of examples, the unanticipated ability of the Day/Night Band (DNB) on the NOAA/NASA Suomi National Polar-orbiting Partnership environmental satellite to resolve gravity structures near the mesopause via nightglow emissions at unprecedented subkilometric detail. On moonless nights, the Day/Night Band observations provide all-weather viewing of waves as they modulate the nightglow layer located near the mesopause (~90 km above mean sea level). These waves are launched by a variety of physical mechanisms, ranging from orography to convection, intensifying fronts, and even seismic and volcanic events. Cross-referencing the Day/Night Band imagery with conventional thermal infrared imagery also available helps to discern nightglow structures and in some cases to attribute their sources. The capability stands to advance our basic understanding of a critical yet poorly constrained driver of the atmospheric circulation.

Suomi NPP | VIIRS | Day/Night Band | nocturnal observations | airglow

Gravity waves (1) play a central role in the atmospheric circulation (2–4) at space and time scales ranging from regional weather to global climate (5). The momentum imparted by wave breaking modulates the upper atmospheric wind flow, which in turn influences weather and climate patterns through myriad coupling processes (6). Examples include the Quasi-Biennial Oscillation, which modulates monsoonal precipitation (7) and mid-latitude storm tracks (6), the Brewer–Dobson circulation, which governs stratospheric ozone transport, and the Semi-Annual Oscillation, which links to the El Niño Southern Oscillation (8) and to high-latitude climatology (9). These waves also influence the formation and properties of polar stratospheric clouds (10). Wave-induced disturbance of ionospheric structure (11) impacts global positioning system (GPS) performance, linking these remote waves to practical aspects of everyday life.

Addressing the high uncertainties in the atmospheric circulation response to external forcing (12) will require better abilities to model the fully coupled system. Improved representation of gravity wave forcing mechanisms, global distribution, space/time evolution, and momentum deposition processes is of prime importance to middle-to-upper atmospheric circulation (13, 14). As numerical models extend their upper bounds (>100 km) and increase their horizontal spatial resolution to capture the full circulation, they are beginning to resolve the subgrid-scale details of mesospheric waves (15). However, these numerical models lack the observations necessary to constrain and improve upon gravity wave drag parameterizations, resulting in possible misrepresentation of important gravity wave processes. Hence there is a clear and pressing need for high-resolution, global observations of the transient and episodic gravity wave spectrum reaching the upper atmosphere (16). Whereas satellite-based measurements have helped to construct a global climatology of gravity waves in the middle stratosphere (30–40 km), such detailed global information about waves reaching the upper mesosphere is unavailable (17, 18). The data gap has limited substantive progress in a critical area.

Here we show how the nadir-viewing Day/Night Band (DNB) radiometer on the *Suomi* National Polar-orbiting Partnership (NPP; hereafter, *Suomi*) satellite (19) holds promise for beginning to fill this gap, offering a unique ability to resolve the fine-scale horizontal structure (at ~0.74-km resolution) of gravity waves near the mesopause (~90 km) globally via sensing of nocturnal atmospheric airglow (or "nightglow"; 20) emissions on moonless nights. We present representative DNB imagery examples of waves launched by a variety of physical mechanisms: isolated and organized convection, topography, jet instabilities, and a volcanic eruption. This windfall capability arises from the DNB's extreme sensitivity to low-level light and holds potentially

Significance

As an unforeseen windfall of its high sensitivity, the Day/Night Band (DNB) low-light visible sensor carried on the Suomi satellite enables global detection of gravity waves in the upper atmosphere at unprecedented subkilometric detail. On moonless nights, the observations provide all-weather viewing of waves as they modulate the nightglow layer located near the mesopause. These waves are launched by a variety of mechanisms ranging from orography to convection, intensifying fronts, and seismic and volcanic events. Wave energy is recognized as the principal driver of upper atmospheric circulation, which in turn influences tropospheric weather patterns. For lack of global observations, information about upper atmospheric wave distribution and character is limited. Here, the DNB begins to fill a critical gap.

Author contributions: S.D.M. designed research; S.D.M. and W.C.S. performed research; S.D.M., W.C.S., J.Y., S.M.S., M.J.A., L.H., M.S., and P.T.P. analyzed data; S.M.S. supplied Fig. S2; M.J.A. helped analyze winds for Fig. 1; L.H. provided information for Fig. 3; M.S. provided Fig. S3; P.T.P. supported analysis of Fig. 1 and Fig. S1; W.C.S. assisted with data acquisition and primary figure preparation; J.Y., S.M.S., M.J.A., L.H., M.S., and P.T.P. assisted with technical review, analysis, and supplementary information; and S.D.M. wrote the paper.

The authors declare no conflict of interest.

This article is a PNAS Direct Submission.

Freely available online through the PNAS open access option.

[1]To whom correspondence should be addressed. Email: steven.miller@colostate.edu.

This article contains supporting information online at www.pnas.org/lookup/suppl/doi:10.1073/pnas.1508084112/-/DCSupplemental.

broad implications for model handling of a key atmospheric energy transfer process.

Wading into the Deep End of the Atmospheric Wave Pool

Earth-viewing satellites provide the best means of yielding global observations of high-altitude gravity waves. Since the 1960s, satellites have characterized gravity wave distributions in the middle atmosphere (21–23). Whereas nadir-viewing infrared sounders, which offer much higher horizontal spatial resolution (~10 km) than limb sounders and GPS radio occultation systems (~100 km), have provided a global climatology of stratospheric gravity waves, corresponding high-resolution observations of waves occurring at mesospheric levels and above have not been available on a regular basis.

Nightglow offers a unique perspective on gravity waves that reach higher altitudes—with strongest emissions near the 85- to 95-km mesopause region. As waves forced by various mechanisms in the lower atmosphere propagate through the middle atmosphere, they will break (sometimes forming secondary waves), be absorbed, reflected, ducted, or pass through according to complex interactions determined by wave properties and the profile of temperature and wind (6). Propagation times can vary greatly depending on wave frequency and wave-relative winds, but typical values of troposphere-to-mesopause times are on the order of 1 h (24)—implying that meteorological sources (e.g., thunderstorms) may have evolved considerably before the first signs of waves appear in the nightglow. As gravity waves pass through or are ducted along the mesopause, they perturb the local temperature and density, modulating the intensity of nightglow emissions occurring there. The result is a signature of the waves themselves through rippling patterns of visible light.

A host of legacy satellite systems (25–28) has provided coarse-resolution descriptions of airglow structure with information mainly on low-amplitude, long-wavelength gravity waves. Among them, the OGO-4 satellite (29) was the first to collect information on broad-scale (~1000-km) regions of enhanced nightglow. However, these previous systems failed to capture the finer-scale structures (<500 km) that are of prime interest to model validation and parameterization needs. Doing so requires high-resolution nadir-viewing systems, capable of contending with much weaker (smaller optical paths) nightglow signals and possible background light contamination.

The current state-of-the-art in nightglow measurement is the Ionosphere, Mesosphere, upper Atmosphere, and Plasmasphere mapping mission (IMAP; 30) flying on the International Space Station. IMAP carries a Visible and near-Infrared Spectrographic Imager (VISI), a 45° fore/aft nadir-viewing radiometer that observes mesoscale nightglow features in multiple bands and at horizontal spatial resolution ranging from 16 to 50 km. This system approaches what is needed to capture fine-scale gravity wave structures from the equator up to midlatitudes (+/−51°). Beyond the 3-y IMAP/VISI mission, however, the community is left with few options for accumulating a long-term global description of the full upper atmospheric gravity wave spectrum.

Suomi Makes a Splash with Global Nightglow Imagery

The NOAA/NASA *Suomi* satellite has produced a "cannonball splash" of sorts into the atmospheric wave pool. Launched on 28 October 2011 as the first of NOAA's next-generation Joint Polar Satellite System (JPSS) operational program, *Suomi* flies in an 834-km altitude Sun-synchronous orbit (~102-min orbital period) with local equatorial crossing times of ~0130 PM (ascending) and 0130 AM (descending). It carries a Day/Night Band (DNB) sensor as part of its Visible Infrared Imaging Radiometer Suite (VIIRS). The DNB is optimized for imaging the nocturnal surface and lower atmosphere at extremely low levels of light within its 505- to 890-nm band pass (19). An unanticipated advantage of its sensitivity is an ability to detect nightglow emissions on moon-free, astronomically dark nights (31) from its 824-km vantage point. The signals, ranging from 10^{-5} to 10^{-7} W m^{-2} sr^{-1} (~100 times fainter than substantially moonlit scenes) manifest both as direct upwelling emission and reflection by underlying clouds and the surface. Thermal infrared window bands included on VIIRS provide a means for decoupling the two components.

The DNB captures the fine-scale details of gravity waves at unprecedentedly high horizontal spatial resolution (742 m across a 3000-km-wide swath). The sensor collects data via a whiskbroom-scanning pattern using 16 detectors, with scans oriented perpendicular to the direction of satellite motion. Each scan of this detector stack forms an ~12-km in-track swath, and adjacent scans are ~1.78 s apart. The horizontal spatial resolution of DNB imagery is maintained at a value of ~0.74 km across the entire swath (i.e., from nadir to scan edge) via a scan-angle-dependent subpixel aggregation strategy. The ability of the DNB to resolve short horizontal wavelengths is important because it is believed that these waves carry most of the vertical flux of horizontal momentum. In terms of vertical resolution, the DNB's ability to detect nightglow waves is governed by the optical path through a geometrically thin (~10 km) layer of nightglow (comprised of emissions from atomic oxygen, sodium, and hydroxyl radicals) located near the mesopause. Similar to ground-based airglow imagers, this finite emission layer geometry provides detection of vertical wavelengths of >10 km. Owing to *Suomi*'s polar-orbiting geometry and the DNB's large swath width, additional coverage from adjacent, overlapping orbital passes increases with increasing latitude.

The waves are launched by a variety of different mechanisms (4), including topography, convection, fronts, jet imbalance (32), wind shear, and secondary wave generation (33). When coupled with atmospheric dissipation processes, these mechanisms yield a wide array of wave characteristics, appearing at times as distinct and regular patterns of alternating bright and dark bands and at other times as very complex patterns arising from wave interactions. The examples to follow provide a sampling of the diverse gravity wave structures seen in DNB nightglow imagery and point toward the potential of these unique observations to address critical gaps in current knowledge, resolving the high-amplitude, shorter-wavelength details of the gravity wave spectrum residing above the stratosphere.

Orography. Gravity waves associated with flow over orography (mountain waves) are an important seasonal source of upper atmospheric energy (34). Global statistics on stratospheric waves from AIRS (18) show seasonally dependent regions of wave generation linked to both major barriers (e.g., the Rocky Mountains of North America, the Andes of South America, the Antarctic Peninsula, and the Himalayas) and isolated features (e.g., South Georgia Island and the Kerguelen Islands in the Southern Ocean; 35). In some cases, particularly during winter, large-amplitude mountain waves reach the mesosphere (36). The DNB begins to answer long-standing questions regarding what fraction of the mountain wave distribution survives the traverse of the stratosphere to reach and influence the upper atmospheric circulation and chemistry.

Many of the world's most important sources of mountain waves are remote and thus poorly observed by surface-based instrumentation. An example of nightglow gravity waves above the Himalaya Ridge and Tibetan Plateau is shown in Fig. 1 (with accompanying analysis in Fig. S1). Without time-resolved observations to confirm a terrain-locked wave pattern, we considered the local wind field as a way of asserting these features to be mountain waves. Winds from European Centre for Medium-range Weather Forecasts (ECMWF), National Centers for Environmental Prediction (NCEP), and Modern-Era Retrospective Analysis (MERRA) model reanalyses near ridge tops are southwesterly and perpendicular to the observed wave crests. Given the observation of westerly stratospheric winds in this region, the

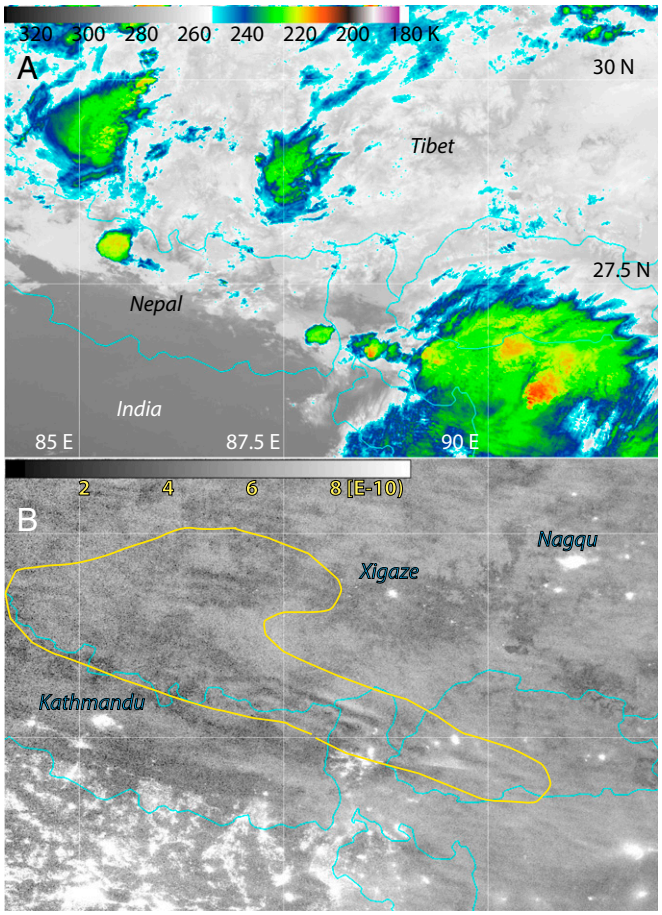

Fig. 1. Gravity waves possibly associated with orography. (*A*) VIIRS thermal infrared (10.76 μm) imagery of the Himalayas and the Tibetan Plateau on 3 May 2014 at 1922 UTC. (*B*) Corresponding Day/Night Band visible/near-infrared imagery, revealing a linearly oriented train of gravity waves (roughly northwest/southeast-oriented bands in the central portion of the image contained in yellow contour, aligned with the local Himalayan ridgeline) over southern Tibet. Bright patches in the southern portions of *B* are city lights from various Indian districts, and distinct cities in Nepal and Tibet are indicated.

model data support the possibility that these are mountain waves. The waves are far removed from the bright city lights emanating from the densely populated Indian districts. VIIRS thermal infrared imagery (Fig. 1*A*) shows the location of meteorological clouds in the scene, which is useful in cross-referencing with DNB nightglow imagery (Fig. 1*B*) to identify the wave structures visually. Observations of mountain waves over this largely inaccessible area are rare. The top-down satellite perspective provides a far more practical means to gathering the information remotely.

Moist Convection. Thunderstorms trigger a broad spectrum of gravity waves via latent heat release and interactions with the mean flow (37). In the early spring and fall, when wind speeds and shear in the middle atmosphere are at a climatological minimum (38), the initial structure of the waves is preserved, resulting in concentric rings of nightglow (39). Fig. 2 shows an example of DNB-observed concentric gravity waves associated with a nocturnal thunderstorm in southern Texas. These ripples of enhanced nightglow, verified by surface networks (Fig. S2), continue well beyond the extent of the storm's anvil clouds (seen via reflection of downwelling nightglow). Typical wavelengths for such events fall in the range of ∼20–30 km. In the presence of wind shear, the rings are morphed into asymmetric, banded, or linearly oriented patterns (40). The DNB provides a more complete picture of these structures than surface-based systems, particularly for cloudy scenes or remote regions (e.g., Fig. S3, which shows similar waves launched by a strong cell over Bangladesh, coupled with surface photography of the event).

The organized convection of tropical cyclones triggers waves observable in nightglow as well (41, 42). Fig. 3 shows an example of waves associated with Hurricane Ana near Hawaii. The DNB imagery reveals a series of westward propagating waves advancing ahead of the system. Concurrent (within 15 min) AIRS-derived temperature perturbations show similar wave structures reside in the midstratosphere at this time. The emergence of these waves gives clues to the timing of latent heat release and insight on evolving warm core dynamics, including storm organization and cycling (43), whereas their geometric structure holds further information about the above-storm environment. Wind shear and wave-absorbing layers of the atmosphere can modulate the waves into linear and even banded patches that appear vastly different from the concentric patterns seen in Figs. 1 and 2 (e.g., wave structures atop Hurricane Hellen, Fig. S4)—relationships between wave morphology and storm behavior/evolution are science questions now enabled by these high-resolution DNB observations.

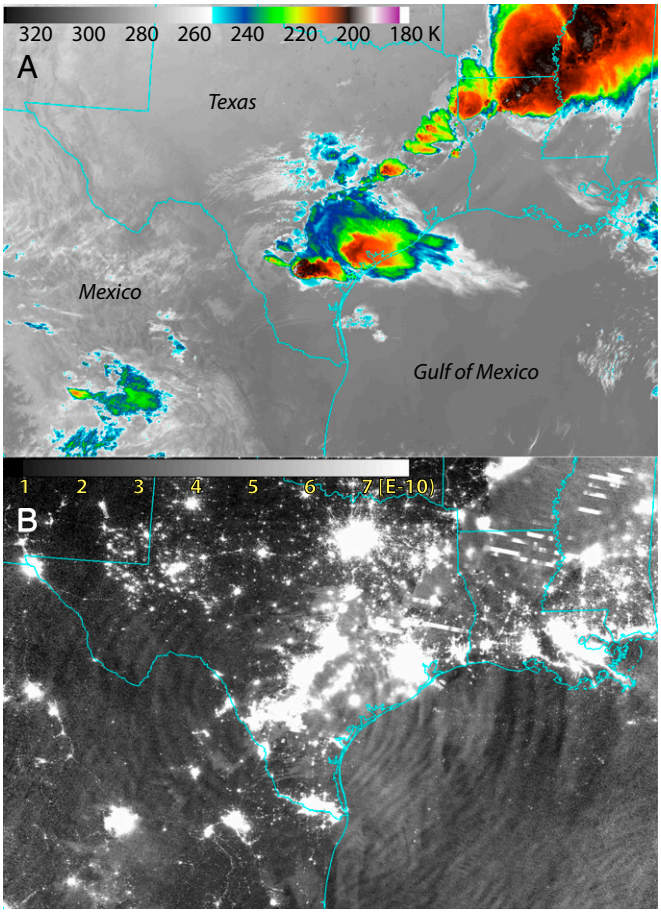

Fig. 2. Concentric gravity waves forced by thunderstorms. (*A*) VIIRS thermal infrared brightness temperatures (10.76 μm) show a line of thunderstorms in southern Texas on 4 April 2014 at ∼0815 UTC (0215 AM, local time). Coldest cloud tops (red, into black) denote deep convection and clouds overshooting the tropopause. (*B*) Corresponding nightglow imagery from the DNB. Amid bright patches of light from various cities and rectangular-shaped streaks caused by lightning flashes during the DNB scans, a well-defined concentric-ring pattern emanates from the southern storms.

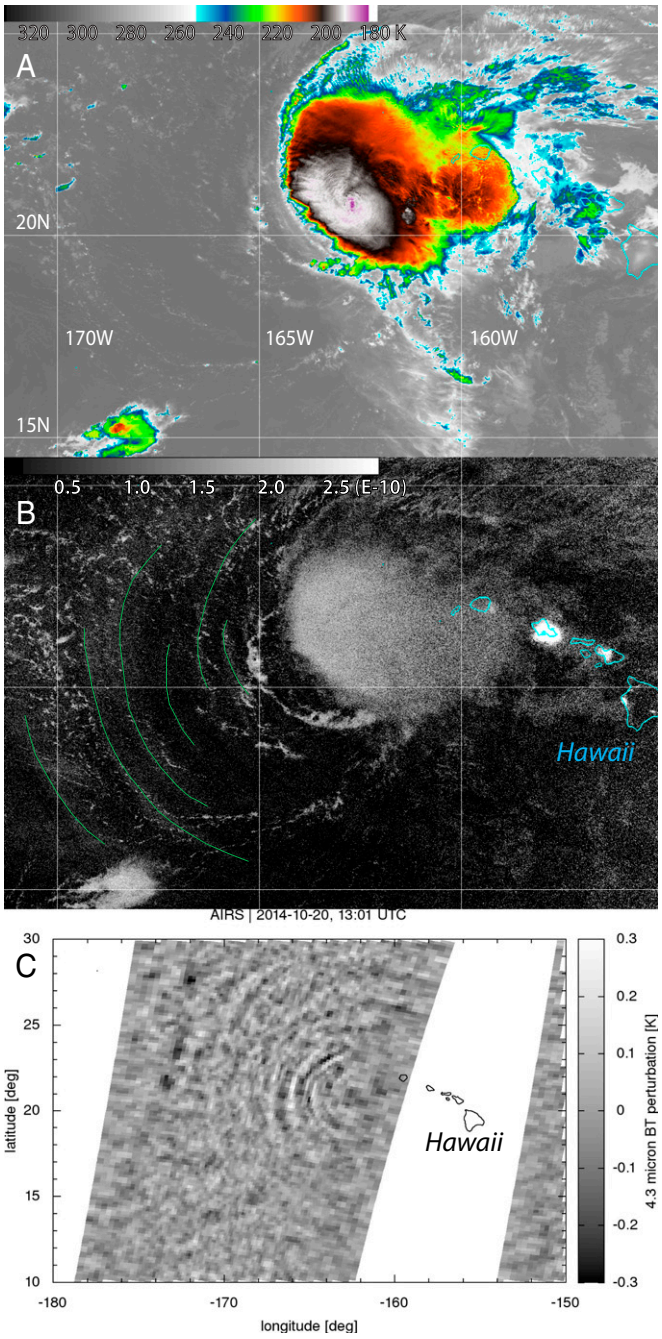

Fig. 3. "Wave sounding" above tropical storm. Strong convection associated with tropical cyclones produces detectable signatures in nightglow. VIIRS thermal infrared imagery (*A*; 10.76 μm) shows Hurricane Ana on the night of 20 October 2014 at 1255 UTC, having passed just to the southwest of the Hawaiian archipelago. Corresponding Day/Night Band imagery (*B*) shows a series of nightglow rings (green curves align with wave-phase fronts) propagating away from the system. The same pattern of rings is noted in AIRS 4.3-μm imagery from Aqua (*C*) at nearly the same time (1310 UTC), which detects temperature perturbations at the 30- to 40-km level. Together, AIRS and the DNB begin to supply a sounding of atmospheric gravity wave activity.

Jet Instabilities. Processes related to jet imbalance and wind shear instability associated with the strong, rapidly evolving jet streams of intensifying cold fronts are well-known sources for gravity waves (32, 44). Although typically weaker than their orographic cousins, the aggregate contribution of these gravity waves to the global distribution of energy and momentum flux may be comparable (45). However, the exact mechanisms responsible for wave launching are not well understood and are difficult to evaluate without a robust observational database. Due to the large spatial extent of jet streams and the extensive cloud cover often associated with them, only a very limited collection of surface-based gravity wave observations exists (46). Here, the DNB's unobstructed top-down view can begin to close the wide observational gap.

Fig. 4 shows gravity waves generated in association with a strong wintertime midlatitude storm system. At the time of the *Suomi* overpass, the low-level central circulation of this system (seen by clouds reflecting downwelling nightglow in Fig. 4*A*) is offshore of the central coast of California. To the west and in the cold sector of the storm, strong northerly winds are seen to orient low-level clouds into "streets" along the flow. DNB-observed gravity waves in nightglow (Fig. 4*A*, within green contour) are seen to orient transversely to the jet stream flow, which included a model-analyzed 140-kt (72 m/s) core jet streak (Fig. 4*B*). In this way, the DNB provides unique information on the detailed morphologies of mesospheric gravity waves occurring over the world's large oceanic basins.

Upper Atmospheric Dynamics. Many DNB-observed nightglow wave features have no obvious ties to lower atmospheric forcing (e.g., Fig. S5). Internal undular bores occurring near the mesopause

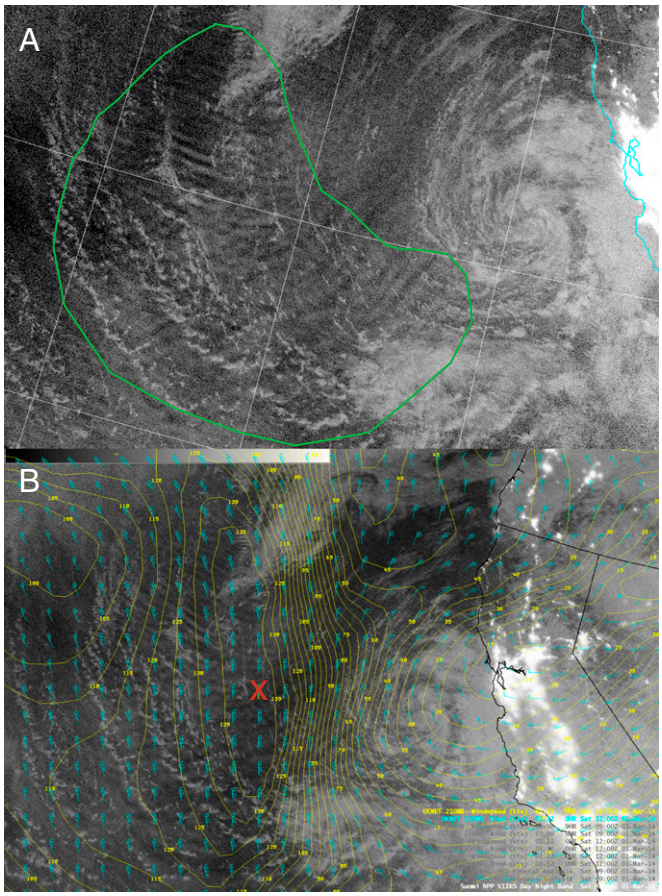

Fig. 4. Waves excited by jet stream dynamics. (*A*) Wave patterns in the nightglow oriented transversely to the tropospheric flow (enclosed in green contour) superimposed upon clouds reflecting the down-welling diffuse nightglow. (*B*) Overlays of 250-mb wind barbs and isotachs at 5-kt intervals (red "X" denotes approximate location of 140-kt jet streak maximum wind speed). U.K. Met Office analysis.

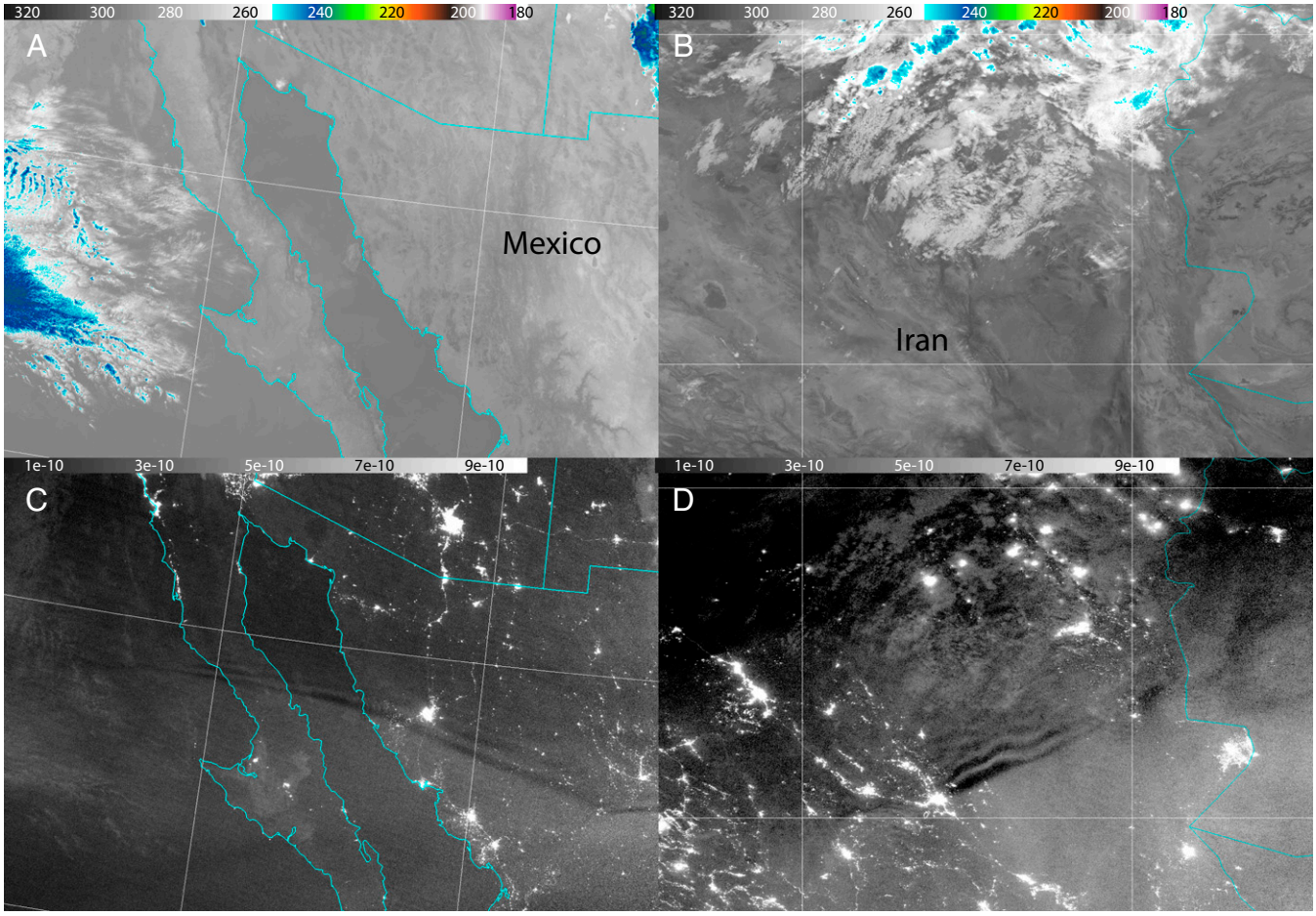

Fig. 5. Mesospheric bores revealed in nightglow. (*A* and *B*) VIIRS 10.76 μm thermal infrared and (*C* and *D*) corresponding Day/Night Band nightglow imagery showing mesospheric bore structures crossing over the Baja California region on 27 February 2014 at ∼0930 UTC and western Iran on 18 November 2014 at ∼2215 UTC. In both cases, the very well defined nightglow wave patterns are oriented linearly along the trailing edge of these southward propagating bores, with the discontinuity between the wave train and the diffuse bright region demarcating the location of the hydraulic jump.

produce a readily identifiable signature in nightglow emissions (47). From a surface observer's perspective, the visual appearance of a bore's passage entails a sudden brightening of the night sky (the "bright night" effect; 48), followed by a sharp wave front associated with the hydraulic jump, and finally a series of linearly oriented alternating bright and dark bands (49). This trailing wave pattern, the bore's principle mechanism for energy dissipation, is phase-locked to the hydraulic jump.

Fig. 5 shows examples of classic bore-induced nightglow signatures seen in DNB imagery over Mexico and Iran. Consistent with the idealized structure described above, the southward propagating bores appear as broad, diffuse regions of elevated nightglow brightness to the south (the "bright night"), followed by sudden discontinuity (the hydraulic jump) and a series of sharply defined east/west-oriented waves trailing off to the north. With its high spatial resolution and wide swath, the DNB provides a fully contiguous synoptic-scale view of these important energy dissipation processes occurring worldwide in the upper atmosphere.

Seismic and Volcanic Activity. The examples above have followed a "ground-up" progression of wave-launching mechanisms (from orography, to convective systems and dynamics of the troposphere, to processes occurring in the upper atmosphere). It seems only fitting to close this discussion by returning to terra firma and noting the remarkable teleconnections that can occur between the tenuous upper atmosphere and geophysical processes of the solid earth. Although the 2011 Tōhoku Earthquake and tsunami in Japan occurred over 8 mo before first light imagery from the DNB, surface-based sensors in Hawaii detected a wave train associated with the propagating tsunami, pointing toward a potential role of spaceborne nightglow sensing in detection and early warning (50). The DNB data are being monitored for seismic-related nightglow stimulation.

If tsunami-generated disturbances on the order of only a few centimeters in amplitude can elicit a nightglow response, it stands to reason that powerful point-source events such as volcanic eruptions might do the same. The DNB finally confirmed this hypothesis on 23 April 2015, the first to our knowledge known spaceborne measurement of its kind, when Chile's Calbuco volcano erupted in Plinian fashion, ejecting an ash plume into the stratosphere and forming a concentric-ring gravity wave pattern in the nightglow above the eruption site. The structure of the waves is reminiscent to that formed by strong tropospheric convection. Fig. 6 shows the *Suomi* perspective on the ash plume and corresponding nightglow wave pattern emanating from the Calbuco volcano epicenter. In its ability to detect pyroclastic flows via light emission, ash plumes via lunar reflectance (19), and, as now shown, perturbations to the nightglow layer during strong eruptions, the DNB offers a powerful assortment of monitoring and diagnostic tools.

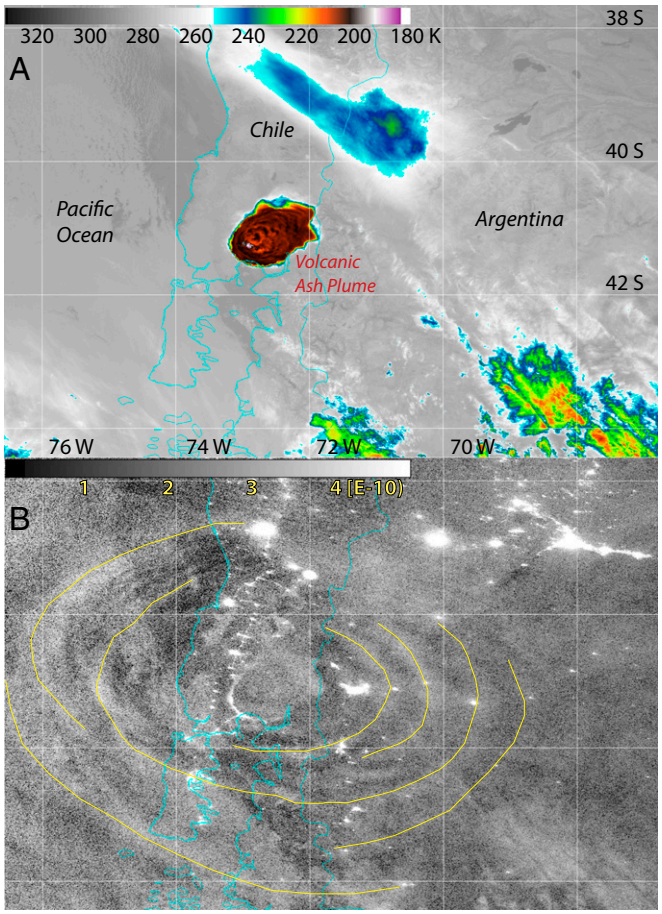

Fig. 6. Volcanic eruption waves. (*A*) VIIRS 10.76 μm thermal infrared imagery showing a deep (cold-top) ash plume atop the erupting Calbuco volcano in Chile on 23 April 2014 at ∼0509 UTC and (*B*) corresponding Day/Night Band nightglow imagery reveal a concentric gravity wave ring pattern (yellow curves align with selected wave-phase fronts) centered on the volcano. The pattern is reminiscent of those observed atop strong midlatitude thunderstorms.

Interpretational Caveats

As the DNB was never designed with nightglow imaging in mind, the observations are not optimized to such applications. This presents several challenges to interpretation and quantitative algorithms for wave identification and warrants a tempered discussion of the limitations. The first of these involves the weakness of signal. Nightglow emissions reside typically 1–2 orders of magnitude below the notional minimum detectable signal of the DNB (defined for a signal-to-noise ratio >5 at scan edge). When analyzing signals so very close to the noise floor, artifacts considered as negligible within the context of the scoped DNB applications become important factors. Differences in the response between the DNB's detectors produce striping patterns oriented along the cross-track scan direction. Small timing errors in the data collection give rise to regular patterns that are most prominent near scan edge. Departures from the prelaunch calibration coefficients produce a false limb brightening that requires monthly adjustment. Stray light contamination (unshielded sunlight leakage into the VIIRS optical assembly which feeds into the DNB) produces a scan-line–oriented brightening near *Suomi*'s day/night terminator crossings that migrates meridionally with the seasons. Software corrections have been introduced to mitigate for these effects, but some residual artifacts remain. Scan geometry and interpretive vigilance near the scan edge and in the stray light zones suffices in most cases for distinguishing visually between true signal and artifact.

As seen in most of the examples, the nightglow gravity wave features are often superimposed upon much stronger background signals. As the DNB was designed for cloud and surface imaging, it senses in a clean spectral window of high atmospheric transmittance (∼80–90%). This presents specific challenges to isolating nightglow features riding atop various reflective and emissive sources in the lower atmosphere and at the surface. Meteorological clouds and high-albedo surfaces reflect downwelling nightglow. These features are discernible in most of the DNB imagery examples shown here. Additionally, anthropogenic lighting (cities, roadways, ship lights, and gas flares) and transient sources of natural light from lightning flashes, fires, and aurora at higher latitudes dominate the signal whenever they are present, obscuring any faint nightglow gravity wave features. The wave features also fade in the vicinity of aurora.

Typical DNB nightglow imagery is thus far more complex than measurements collected in parts of the spectrum where the lower atmosphere is opaque or for surface-based, upward viewing systems where information on the position of individual stars and the diffuse brightness of the Milky Way are well inventoried. Whereas the wave structures are plainly evident to the human eye, extracting them via objective pattern recognition algorithms and filters poses a greater challenge. Simple background subtraction, a standard practice for the atmospherically opaque bands of AIRS (18) and for upward pointing terrestrial systems, is only possible for a small subset of DNB observations collected over relatively cloud-free oceanic scenes. Algorithms based on 2D Fourier Transform image analysis and enlisting information on the background cloud cover, surface type, and stable terrestrial lights are currently in development for the DNB.

Finally, there is the limitation of temporal sampling. Nightglow imaging from the DNB is possible only in the astronomically dark portion of *Suomi*'s orbit (solar zenith angles exceeding 109° so as to avoid contamination by twilight). This precludes diurnal sampling of wave activity. Furthermore, not all astronomically dark nights offer sufficiently low background; moonlit scenes may exceed 100 times that of nightglow emissions, thus saturating any gravity wave details. The data collections are thus limited to moonless nights, which for the *Suomi* orbit corresponds to a ∼2-wk period spanning roughly two nights after Last Quarter until two nights after First Quarter lunar phase. During these periods, nightglow gravity wave structures appear regularly within DNB imagery. However, we are left with corresponding ∼2-wk gaps defined by the ∼29.5-d lunar cycle. Per the geometry of the seasons and day length, at high latitudes there are prolonged gaps in nightglow monitoring in the summer, with corresponding periods of sustained coverage in the winter.

Glowing Ripple Effect—Lighting a Path Ahead

Suomi's DNB has exhibited an unexpected capability to detect gravity waves occurring globally at the mesopause via nightglow emission signatures for moonless nighttime scenes. A unique advantage of the DNB is its ability to resolve subkilometer-scale structural details of waves that typically cannot be observed regularly from the surface due to cloud obscuration, their spatial extent, or their remote nature. In this way, the DNB helps to address a key observational gap. Whereas their utility for improving model gravity wave parameterizations in the near-term is unlikely, these observations will at a minimum tell more about the distribution and character of mesospheric gravity waves. The long-term compilation of DNB data from both *Suomi* and the forthcoming JPSS constellation members (a series running through 2025) holds greater promise to improve our general understanding of wave-energy impacts on general circulation and climate.

Formalizing and advancing this demonstrated nightglow capability (among the myriad other utilities of nighttime visible-light

sensing) on next-generation satellite observing systems warrants consideration. A disadvantage of the DNB with respect to surface systems is a background complicated by terrestrial light reflection and emission signals. Whereas the DNB's spectral response offers partial overlap with the spectrum of nightglow emission, stronger hydroxyl emissions in the Meinel band reside at slightly longer wavelengths of the near-infrared. A nadir-viewing instrument of similar or improved sensitivity to the DNB, tuned to the nightglow emissions, would further improve detection. Such a sensor could take advantage of the relatively opaque water vapor absorption bands located near 1.15, 1.40, and 1.85 μm to suppress contributions from reflective and nonnightglow emissive sources in the lower atmosphere and at the surface, simplifying the task of wave identification.

As noted, a key limitation of the DNB on its current platform is poor temporal sampling. Due to Suomi's Sun-synchronous polar orbit, low to midlatitude regions receive only 1–2 observations per night. DNB nightglow imagery provides only a snapshot of the ephemeral scene and thus cannot describe the details of fine-scale wave propagation. Time-resolved information on the order of 1–10 min is necessary to characterize adequately the evolution and phase speed of the waves and understand wave interactions within the upper atmosphere (39). A future geostationary-based system—one coupling nightglow-sensitive visible/near-infrared with the middle-wave infrared bands used for stratospheric wave detection—would enable high temporal sampling and a true quantum leap in our ability to characterize the 3D, transient behavior of upper atmospheric gravity waves. Such a system would also expand the portions of nights observable under astronomically dark conditions.

The caveats mentioned above do little to temper the excitement surrounding the potential for these new observations to make an impact. At this very early stage, the DNB's unforeseen capabilities resemble more of a diamond in the rough—a raw but promising nuance to measurements collected on the darkest nights. Even so, this nightglow wave imagery already sparkles with potentially valuable information content. A global, statistical analysis of the multiyear time series of DNB nightglow imagery amassed to date is an important next step to capitalizing on this opportunity. With refinement and further advances to satellite-based low-light technology, we may one day look back and regard the DNB not only as a gem in its own right, but as part of the foundation to our understanding of the full atmospheric circulation.

ACKNOWLEDGMENTS. Support of the National Oceanic and Atmospheric Administration Joint Polar Satellite System Proving Ground and Risk Reduction Program (Grant NA14OAR4320125 Amd 7) and the Naval Research Laboratory (Grant N00173-14-G902), as well as the Oceanographer of the Navy through its office at the Program Executive Office for Command, Control, Communications, Computers and Intelligence & Space/PMW-120 under Program Element PE-0603207N, is gratefully acknowledged.

1. Holton JR (1992) *An Introduction to Dynamic Meteorology* (Academic Press, London), 3rd Ed.
2. Lindzen RS (1981) Turbulence and stress owing to gravity wave and tidal breakdown. *J Geophys Res* 86(C10):9707–9714.
3. Holton JR (1982) The role of gravity wave induced drag and diffusion in the momentum budget of the mesosphere. *J Atmos Sci* 39(4):791–799.
4. Fritts DC, Alexander MJ (2003) Gravity wave dynamics and effects in the middle atmosphere. *Rev Geophys* 41(1):1003.
5. McLandress C, Shepherd TG, Polavarapu S, Beagley SR (2012) Is missing orographic gravity wave drag near 60°S the cause of the stratospheric zonal wind biases in chemistry-climate models? *J Atmos Sci* 69:802–818.
6. Alexander MJ, et al. (2010) Recent developments in gravity wave effects in climate models, and the global distribution of gravity wave momentum flux from observations and models. *Q J R Meteorol Soc* 136:1103–1124.
7. Meehl GA (1991) A re-examination of the mechanism of the semiannual oscillation in the southern hemisphere. *J Clim* 4:911–926.
8. Li T, et al. (2013) Influence of El Niño-Southern Oscillation in the mesosphere. *Geophys Res Lett* 40:3292–3296.
9. Van den Broeke M (2000) The semi-annual oscillation and Antarctic climate. Part 3: The role of near-surface wind speed and cloudiness. *Int J Climatol* 20:117–130.
10. Eckermann SD, Hoffmann L, Höpfner M, Wu DL, Alexander MJ (2009) Antarctic NAT PSC belt of June 2003: Observational validation of the mountain wave seeding hypothesis. *Geophys Res Lett* 36:L02807.
11. Hernández-Pajares M, Juan JM, Sanz J (2006) Medium-scale traveling ionospheric disturbances affecting GPS measurements: Spatial and temporal analysis. *J Geophys Res* 111:A07S11.
12. Shepherd TG (2014) Atmospheric circulation as a source of uncertainty in climate change projections. *Nat Geosci* 7:703–708.
13. Richter JH, Sassi F, Garcia RR (2010) Towards a physically based gravity wave source parameterization in a general circulation model. *J Atmos Sci* 67:136–156.
14. McLandress C, Scinocca JF (2005) The GCM response to current parameterizations of nonorographic wave drag. *J Atmos Sci* 62:2394–2413.
15. Preusse P, et al. (2014) Characteristics of gravity waves resolved by ECMWF. *Atmos Chem Phys* 14:10483–10508.
16. Geller MA, et al. (2013) A comparison between gravity wave momentum fluxes in observations and climate models. *J Clim* 26:6383–6405.
17. Gong J, Wu DL, Eckermann SD (2012) Gravity wave variances and propagation derived from AIRS radiances. *Atmos Chem Phys* 12:1701–1720.
18. Hoffmann L, Xue X, Alexander MJ (2013) A global view of stratospheric gravity wave hotspots located with Atmospheric Infrared Sounder observations. *J Geophys Res* 118(2):416–434.
19. Miller SD, et al. (2013) Illuminating the capabilities of the Suomi NPP VIIRS Day/Night Band. *Remote Sens* 5:6717–6766.
20. Ingham MF (1971) The light of the night sky and the interplanetary medium. *Rep Prog Phys* 34:875–912.
21. Picard RH, et al. (1998) Remote sensing of discrete stratospheric gravity-wave structure at 4.3-μm from the MSX satellite. *Geophys Res Lett* 25(15):2809–2812.
22. Eckermann SD, Preusse P (1999) Global measurements of stratospheric mountain waves from space. *Science* 286(5444):1534–1537.
23. Alexander MJ, Barnet C (2007) Using satellite observations to constrain gravity wave parameterizations for global models. *J Atmos Sci* 64(5):1652–1665.
24. Yue J, Hoffmann L, Alexander MJ (2013) Simultaneous observations of convective gravity waves from a ground-based airglow imager and the AIRS satellite experiment. *J Geophys Res* 118:3178–3191.
25. Shepherd GG, et al. (1973) An observation of polar aurora and airglow from the ISIS-II spacecraft. *Planet Space Sci* 21(5):819–829.
26. Donahue TM, Guenther B, Thomas RJ (1973) Distribution of atomic oxygen in the upper atmosphere deduced from Ogo 6 airglow observations. *J Geophys Res* 78(28): 6662–6689.
27. Torr MR, Hays PB, Kennedy BC, Walker JCG (1977) Intercalibration of airglow observatories with the Atmosphere Explorer satellite. *Planet Space Sci* 25(2):173–184.
28. Russell JM, III, Mlynczak MG, Gordley LL, Tansock JJ, Jr, Esplin RW (1999) Overview of the SABER experiment and preliminary calibration results. *Proc SPIE* 3756:277–288.
29. Reed EI, Fowler WB, Blamont JE (1973) An atlas of low-latitude 6300-Å [O I] night airglow from Ogo 4 Observations. *J Geophys Res* 78(25):5658–5675.
30. Sakanoi T, et al. (2011) Imaging observation of the Earth's mesosphere, thermosphere and ionosphere by VISI of ISS-IMAP on the international space station. *IEEE Trans. Fundam. Mater* 131(12):983–988.
31. Miller SD, Combs C, Kidder SQ, Lee TF (2012) Assessing global and seasonal lunar availability for nighttime low-light visible remote sensing applications. *J. Ocean. Atmos. Tech* 29(4):538–557.
32. Plougonven R, Zhang F (2014) Internal gravity waves from atmospheric jets and fronts. *Rev Geophys* 52:33–76.
33. Zhou X, Holton JR, Mullendore G (2002) Forcing of secondary waves by breaking of gravity waves in the mesosphere. *J Geophys Res* 107(D7):4058.
34. Carslaw KS, et al. (1998) Increased stratospheric ozone depletion due to mountain-induced atmospheric waves. *Nature* 391:675–678.
35. Alexander MJ, Grimsdell AW (2013) Seasonal cycle of orographic gravity wave occurrence above small islands in the Southern Hemisphere: Implications for effects on the general circulation. *J Geophys Res Atmos* 118(20):11589–11599.
36. Smith S, Baumgardner J, Mendillo M (2009) Evidence of mesospheric gravity-waves generated by orographic forcing in the troposphere. *Geophys Res Lett* 36:L08807.
37. Grimsdell AW, Alexander MJ, May PT, Hoffmann L (2010) Model study of waves generated by convection with direct validation via satellite. *J Atmos Sci* 67:1617–1631.
38. Yue J, et al. (2009) Concentric gravity waves in the mesosphere generated by deep convective plumes in the lower atmosphere near Fort Collins, Colorado. *J Geophys Res* 114:D06104.
39. Taylor MJ, Hapgood MA (1988) Identification of a thunderstorm as a source of short period gravity waves in the upper atmospheric nightglow emissions. *Planet Space Sci* 36:975–985.
40. Vadas S, Yue J, Nakamura JT (2012) Mesospheric concentric gravity waves generated by multiple convection storms over the North America Great Plain. *J Geophys Res* 117: D07113.
41. Suzuki S (2013) Typhoon-induced concentric airglow structures in the mesopause region. *Geophys Res Lett* 40(22):5983–5987.
42. Yue J, Miller SD, Hoffmann L, Straka WC, III (2014) Stratospheric and Mesospheric concentric gravity waves over Tropical Cyclone Mahasen: Joint AIRS and VIIRS satellite observations. *J Atmos Sol Terr Phys* 119:83–90.
43. Dunion JP, Thorncroft CD, Velden CS (2014) The tropical cyclone diurnal cycle of mature hurricanes. *Mon Weather Rev* 142(10):3900–3919.
44. Uccellini LW, Koch SE (1987) The synoptic setting and possible source mechanisms for mesoscale gravity wave events. *Mon Weather Rev* 115:721–729.

45. Hertzog A, Boccara G, Vincent R, Vial F, Coquerez P (2008) Estimation of gravity-wave momentum fluxes and phase speeds from long-duration stratospheric balloon flights. 2. Results from the Vorcore campaign in Antarctica. *J Atmos Sci* 65:3056–3070.
46. Fritts DC, Nastrom G (1992) Sources of mesoscale variability of gravity waves. Part II: Frontal, convective, and jet stream excitation. *J Atmos Sci* 49(2):111–127.
47. Dewan EM, Picard RH (2001) The origin of mesospheric bores. *J Geophys Res* 106: 2921–2927.
48. Bates DR (1960) Bright nights. *Physics of the Upper Atmosphere*, ed Ratcliffe JA (Academic, San Diego, CA), pp 236–237.
49. Smith SM, et al. (2003) A multidiagnostic investigation of the mesospheric bore phenomenon. *J Geophys Res* 108(A2):1083.
50. Makela JJ, et al. (2011) Imaging and modelling the ionospheric airglow response over Hawaii to the tsunami generated by the Tohoku earthquake of 11 March 2011. *Geophys Res Lett* 38:L00G02.